Roles of Barotropic Convective Momentum Transport in the Intraseasonal Oscillation*

FEI LIU

Earth System Modelling Center and Climate Dynamics Research Center, Nanjing University of Information Science and Technology, Nanjing, China

BIN WANG

International Pacific Research Center, and Department of Meteorology, University of Hawai'i at Mānoa, Honolulu, Hawaii

IN-SIK KANG

School of Earth and Environmental Sciences, Seoul National University, Seoul, South Korea

(Manuscript received 10 August 2014, in final form 15 March 2015)

ABSTRACT

Both observational data analysis and model simulations suggest that convective momentum transport (CMT) by cumulus convection may play a significant role in the intraseasonal oscillations (ISO) by redistributing atmospheric momentum vertically through fast convective mixing process. The authors present a simple theoretical model for the ISO by parameterizing the cumulus momentum transport process in which the CMT tends to produce barotropic wind anomalies that will affect the frictional planetary boundary layer (PBL). In the model with equatorial easterly vertical wind shear (VWS), it is found that the barotropic CMT tends to select most unstable planetary-scale waves because CMT suppresses the equatorial Ekman pumping of short waves, which reduces the shortwave instability from the PBL moisture convergence and accelerates the shortwave propagation. The model with subtropical easterly VWS has behavior that can be qualitatively different from the model with equatorial easterly VWS and has robust northward propagation. The basic mechanism of this northward propagation is that the CMT accelerates the barotropic cyclonic wind to the north of ISO, which will enhance the precipitation by PBL Ekman pumping and favor the northward propagation. The simulated northward propagation is sensitive to the strength and location of the seasonal-mean easterly VWS. These results suggest that accurate simulation of the climatological-mean state is critical for reproducing the realistic ISO in general circulation models.

1. Introduction

The intraseasonal oscillation (ISO) with a 30–90-day time scale is an important mode in the tropical atmosphere, which is dominated by the boreal winter Madden–Julian oscillation (MJO) and boreal summer ISO (BSISO). The ISO has large impacts on a wide variety of climate phenomena across different spatial and temporal scales, for example, the onset of some El Niño events (Moore and Kleeman 1999; Zhang 2005), the Pacific–North American (PNA) pattern (Mori and Watanabe 2008), and the Arctic Oscillation (Zhou and Miller 2005). The northward propagation of the BSISO is closely related to the active and break periods of the Indian summer monsoon (Annamalai and Slingo 2001).

The ISO always appears as a planetary-scale oscillation, and many studies have been carried out to explain this scale selection. For example, the longwave approximation in the planetary boundary layer (PBL) moisture convergence (Wang 1988; Wang and Rui 1990), the role of nonlinear heating in the Rossby–Kelvin wave system coupled by the PBL moisture

* Earth System Modeling Center Contribution Number 0042.

Corresponding author address: Dr. Fei Liu, Earth System Modeling Center, Nanjing University of Information Science and Technology, Ningliu Lu, Nanjing 410042, China.
E-mail: liuf@nuist.edu.cn

DOI: 10.1175/JCLI-D-14-00575.1

convergence (Wang and Xue 1992; Li and Zhou 2009), the large surface friction and strong momentum diffusion of the short waves in the troposphere (Kang et al. 2013), the thermodynamics in the moisture mode (Sobel and Maloney 2012, 2013), and the scale interaction between the ISO and synoptic-scale waves (Wang and Liu 2011; Liu and Wang 2012b) all can select the planetary-scale oscillation of ISO.

The ISO also shows prominent seasonal variation (Madden 1986; Wang and Rui 1990; Zhang and Dong 2004; Kikuchi et al. 2012). In the boreal winter, the planetary-scale, eastward-propagating MJO dominates over the tropical Indo-western Pacific (Madden and Julian 1971, 1972). In the boreal summer, the northward-/northeastward-propagating BSISO dominates over the Indian Ocean (Yasunari 1979; Annamalai and Sperber 2005; Wang et al. 2005), and the northward-/northwestward-propagating BSISO dominates over the western North Pacific (Murakami 1984; Kemball-Cook and Wang 2001). The land surface heat fluxes (Webster and Holton 1982), the interaction between convection and moist stability (Gyoswami and Shukla 1984), the air–sea interaction (Kemball-Cook and Wang 2001), the interaction between baroclinic and barotropic vorticity forced by vertical wind shear (VWS) (Wang and Xie 1997; Jiang et al. 2004; Drbohlav and Wang 2005), and the beta shift (Boos and Kuang 2010) mechanisms have been presented to explain this northward propagation of the BSISO. In the ERA-Interim reanalysis and the super parameterized Community Climate System Model (SP-CCSM), the boundary layer moisture advection and the barotropic vorticity effect are found to be the dominant mechanisms for the northward propagation (DeMott et al. 2013).

Convective momentum transport (CMT) is also found to be important for the ISO. Convection not only provides heating to the atmosphere but also redistributes the atmospheric momentum vertically through relatively fast convective mixing processes. The CMT by cumulus convection may be a positive feedback in the MJO, and the kinetic energy is transferred upscale from subgrid systems to the large-scale zonal flow during the westerly onset phase of the MJO (Wu and Yanai 1994; Tung and Yanai 2002a,b). Recently, some general circulation model (GCM) experiments showed that the CMT by cumulus convection is important for the simulation of northward propagation of the BSISO (Kang et al. 2010, hereafter K10), and their results showed that, among the models that Sperber and Annamali once used (Sperber and Annamalai 2008), most models with the CMT are able to simulate the northward propagation, but all of the models without the CMT fail to reproduce the northward-propagating signal. This conclusion, however, needs to be validated by more modeling studying in the future, since many GCMs considering cumulus momentum transport still cannot simulate the northward propagation of the BSISO. In K10, two experiments with and without the CMT were also compared by using the ocean–atmosphere coupled GCM of Seoul National University; the results showed that the experiment with the CMT can simulate the northward propagation of the BSISO while the experiment without the CMT cannot.

To explain why the model with (without) the CMT can (cannot) simulate the northward propagation, K10 presented one mechanism: the lower-level convergence to the north of convection, which is induced by the secondary meridional circulation associated with the baroclinic CMT under the easterly VWS, contributes to this northward propagation. However, the assumption of zonal symmetry in this mechanism cannot represent the role of waves, and the baroclinic CMT-induced northward propagation of the zonally symmetric rainband is too weak; it has a phase speed of $0.2^\circ\,\mathrm{day}^{-1}$ only. In observations, the northward-propagation speed of the ISO is about $0.75^\circ\,\mathrm{day}^{-1}$ over the Indian Ocean (K10). The work of K10 was based on the 2-layer baroclinic framework and the instability in their model was generated by slightly negative moisture static stability, so the role of barotropic mode could not be studied. The CMT by cumulus convection actually has a strong barotropic component (Schneider and Lindzen 1976). While its barotropic structure has also been found in the observation (Oh et al. 2015) and in the model simulation (Miyakawa et al. 2012), the role of barotropic CMT has not been studied before. Thus, we try to understand the role of barotropic CMT by cumulus convection using a theoretical ISO model in this study.

The remainder of the paper is organized as follows. A theoretical 2.5-layer model of the ISO is presented in section 2. This section also introduces the barotropic CMT processes. In section 3, analytical solutions under different easterly VWSs are presented to illustrate the role of CMT. In section 4 the initial value problem has been calculated to study the role of CMT in the northward propagation of the ISO. Some discussion and concluding remarks are given in section 5.

2. The moist wave dynamical model with barotropic CMT

a. *Physical consideration*

The essential dynamics of ISO involves coupling both wave dynamics and moisture processes (Wang and Rui 1990; Wang and Xie 1997; Sobel and Maloney 2012,

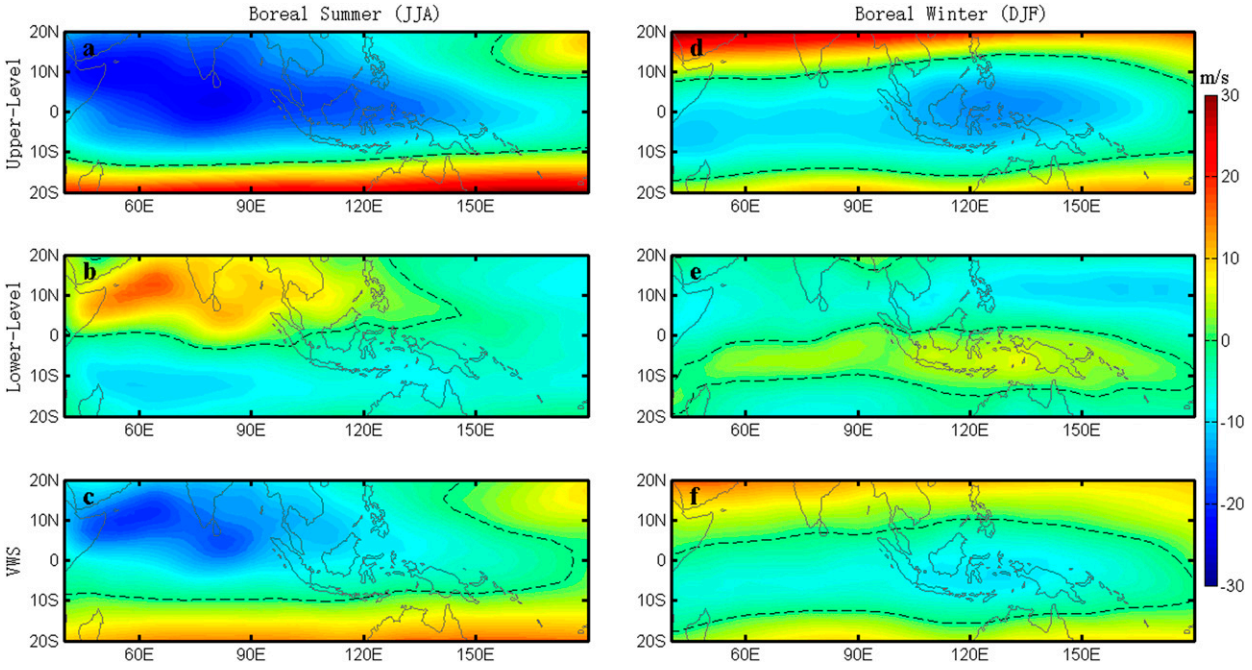

FIG. 1. Observed vertical wind shear (VWS). Shown are climatological mean (1948–2012) upper-level (200 hPa) zonal wind, lower-level (850 hPa) zonal wind, and VWS [(200–850 hPa)/2] for the (a)–(c) boreal summer [June–August (JJA)] and (d)–(f) boreal winter [December–February (DJF)], respectively. Zero wind and zero VWS are denoted by the dark dashed lines.

2013). The theoretical model used in this study is based on the 2.5-layer model (Wang and Rui 1990) and the ISO skeleton model of Majda and Stechmann (Majda and Stechmann 2009), in which the PBL moisture convergence is a moisture source for the free troposphere, and the steady PBL model is used. To represent the moisture processes, we added the tendency of moisture perturbation into the moisture equation. Since the moisture processes are included now, we have to parameterize the precipitation P. In the observation, specifically on the planetary/intraseasonal scales, several studies have shown that the lower troposphere tends to moisten during the suppressed convection phase of the MJO, and that lower-tropospheric moisture leads to MJO's heating anomaly (Myers and Waliser 2003; Kikuchi and Takayabu 2004; Kiladis et al. 2005; Tian et al. 2006). Thus, in the model, the tendency of precipitation is assumed to be proportional to the moisture perturbation q (Majda and Stechmann 2009).

Cumulus convection tends to mix the winds in the vertical direction quickly (Wu and Yanai 1994). In the NCEP/Department of Energy (DOE) Reanalysis II (Kanamitsu et al. 2002), the climatological mean summer (June–September) zonal wind over India and the Indian Ocean region (5°–25°N) has strong upper-level easterly winds and lower-level westerly winds, which gives a strong easterly VWS (Figs. 1a–c). This easterly VWS also exists over the Indo-western Pacific in the boreal winter (Figs. 1d–f). The convection transports momentum to the upper level that has a strong barotropic component (Kang and Held 1986). In this work we mainly focus on the barotropic mode of CMT. Through the parameterization of vertical transport of momentum by cumulus clouds (Schneider and Lindzen 1976), the linear barotropic CMT is proportional to the upward wind anomaly and the seasonal-mean VWS. Under the easterly VWS, the upward (downward) motion of wet (dry) phase of ISO will mix the westerly (easterly) wind of VWS and produces additional barotropic westerly (easterly) wind forcing. Following the parameterization of Kang and Held (Kang and Held 1986), we parameterize the barotropic CMT by assuming that the CMT is proportional to precipitation and VWS (i.e., $\mathrm{CMT} = -sUP$). Here, $s = 1.25$, the dimensional value of which is $0.5\,\mathrm{cm}^{-1}$, and it is reasonable for typical precipitation having a value of $2.4\,\mathrm{mm\,day}^{-1}$ on the intraseasonal time scale (Zhou and Kang 2013). The formula $U = (U_1 - U_2)/2$ denotes the VWS, which is positive (negative) for westerly (easterly) VWS.

b. Model formulation

The seasonal-mean flows are found to be important for the ISO (Wang and Xie 1997; Jiang et al. 2004; Drbohlav and Wang 2005). In a perturbation model

based on balanced mean flow, the seasonal-mean flows should be included in the momentum equations (Wang and Xie 1997). To focus on the role of the barotropic CMT, the advection term that plays a critical role in the northward propagation of ISO is neglected.

In observations, the ISO shows a dominant baroclinic mode with maximum diabatic heating occurring at the midtroposphere and strong circulation at the upper and lower troposphere (Madden and Julian 1972, 1994; Zhang 2005). Without considering the complicated multicloud vertical structure of the ISO, the ISO can be driven by the midtropospheric diabatic heating, which excites a circulation on the first baroclinic mode (Khouider and Majda 2006, 2007). In this 2-layer troposphere model, we assume that diabatic heating only occurs at the midtroposphere. Since the moisture decreases upward exponentially in the tropical atmosphere and is controlled mainly by lower-tropospheric circulation (Wang 1988), its process can be represented by the first baroclinic mode on the lowest-order assumption (Majda and Stechmann 2009). The frictional moisture convergence in the PBL also pumps moisture and moistens the lower troposphere; thus, the Ekman pumping term can be added to the moisture equation (Wang and Rui 1990; Liu and Wang 2012a).

In this simple model, the barotropic and baroclinic modes are defined as $A_+ = (A_2 + A_1)/2$, and $A_- = (A_2 - A_1)/2$, respectively. The subscripts "+, −, 1, and 2" denote the barotropic mode, baroclinic mode, upper level, and lower level, respectively. Taking $C = 50\,\mathrm{m\,s^{-1}}$ (the lowest internal gravity wave speed) as the reference speed, and the characteristic temporal and spatial scales as $\sqrt{1/C\beta} = 8.5\,\mathrm{h}$ and $\sqrt{C/\beta} = 1500\,\mathrm{km}$, where β represents the leading-order curvature effect of the earth at the equator. Thus, the dimensionless equations of baroclinic mode can be written as

$$\begin{aligned} yu_- - T_{-y} &= 0,\\ T_{-t} - u_{-x} - v_{-y} &= P - dT_-,\\ q_{-t} + \tilde{Q}(u_{-x} + v_{-y}) &= -P + r_b(T_s - 9.18)w_b,\\ P_t &= \Gamma q_-, \end{aligned} \tag{1}$$

where u_- and v_- are the zonal (x) and meridional (y) velocities, respectively; T_- is temperature; and w_b is the PBL Ekman pumping, which tends to moisten the low troposphere. The magnitude of the nondimensional vertical gradient of background moisture $\tilde{Q}$ is taken as 0.9, which is the standard value for low-frequency motions (Yano and Emanuel 1991; Frierson et al. 2004). Here $\Gamma \approx 0.018$ ($\approx 0.2\,\mathrm{K^{-1}day^{-1}}$ in dimensional units), which acts as a dynamic growth/decay rate of precipitation, in response to the moisture anomaly. For simplicity, the momentum and thermal damping coefficients take the same value d in the free troposphere, which has a dimensional scale of 5 days. The standard PBL coefficient is $r_b = 0.06\,\mathrm{K^{-1}}$ (Liu and Wang 2012a). The variable T_s is the sea surface temperature (SST) and its magnitude is chosen to be 29°C.

Since the role of mean flow VWS (i.e., the vertical shear mechanism) (Jiang et al. 2004), is neglected, this barotropic CMT will force the barotropic equations directly, which are written as

$$\begin{aligned} u_{+t} - yv_+ - T_{+x} &= \mathrm{CMT} - du_+,\\ yu_+ - T_{+y} &= 0,\\ w_b + u_{+x} + v_{+y} &= 0. \end{aligned} \tag{2}$$

Over the vast area of the ocean, the PBL is well mixed and can be treated as a slab, thus it is reasonable to assume that the PBL temperature anomalies are equal to that at the top of the PBL (i.e., the lower-tropospheric temperature anomalies) in this simple model (Wang 1988; Wang and Li 1994). The PBL friction has a time scale of several hours. For the ISO that has a 30–60-day time scale, the wind tendency in the PBL is small and negligible compared to the friction term, and the steady PBL assumption is reasonable for the intraseasonal time scale (Wang and Li 1993). Observations also show that this steady PBL assumption can well simulate the PBL Ekman pumping of ISO (Salby and Hendon 1994; Hsu and Li 2012). When assuming that the PBL is forced by the lower-level pressure anomalies, the equations for the steady frictional PBL can be simply written as

$$\begin{aligned} Eu_b - yv_b &= \tilde{T}_x\\ Ev_b + yu_b &= \tilde{T}_y, \end{aligned} \tag{3}$$

where the lower-level temperature anomalies $\tilde{T} = T_- + T_+$ and the subscript b denotes the PBL. The Ekman pumping w_b is

$$w_b = -\frac{H_b}{H_T}(d_1\nabla^2\tilde{T} + d_2\tilde{T}_x + d_3\tilde{T}_y), \tag{4}$$

where $d_1 = E/(E^2 + y^2)$, $d_2 = -(E^2 - y^2)/(E^2 + y^2)^2$, and $d_3 = -2Ey/(E^2 + y^2)^2$ (Liu and Wang 2012a). The PBL depth $H_b = 1\,\mathrm{km}$, and the troposphere depth scale is $H_T = 16/\pi = 5.1\,\mathrm{km}$ (Majda and Biello 2004). The PBL friction E is selected to represent damping of half a day. In observation, this equation can well simulate the equatorial Ekman pumping of the ISO (Hsu and Li 2012).

c. Mathematical methods

These linear equations (1)–(4) can be solved as an eigenvalue problem, or they can be integrated from an initial disturbance. After projecting them onto the zonal wavenumber–frequency space, we can obtain the eigenvalues and eigenvectors by matrix inversion. The frequency and growth rate in the eigenvalue problem are defined by the real and imaginary parts of eigenvalues, respectively. Detail of this calculation can be found in Liu and Wang (2012a).

This projection on the zonal wavenumber–frequency space cannot represent the meridional-propagating waves, so we have to solve the initial value problem. To integrate this model, an initial wavenumber-1 Kelvin wave–like perturbation is used. The finite-difference method is adopted in both time and space. The time integration scheme is centrally differenced with a 2.5-min time step and a time-average coefficient of 0.125. For instance, on step n, any variable A_n can be calculated by $A_n = A_n^* + 0.125(A_{n+1}^* + A_{n-1} - 2A_n^*)$, where the subscript denotes the step (number). Here, A_n^* and A_{n+1}^* are calculated from A_{n-1} by the forward difference method. The spatial resolution is 2.5° longitude by 2.5° latitude, and the model domain is from 35°S to 35°N. Sensitivity experiments showed that different grids do not affect the results qualitatively. The zonal boundary condition is periodic around the globe, and the fluxes of mass, momentum, and heat normal to the lateral boundary all vanish.

For the initial value problem, the initial disturbance is set to have the equatorially trapped structure, and the zonal structure is wavenumber 1. The model reaches a steady state from day 30 onward. By this time, initial transient features have decayed, leaving nearly periodic disturbances that are close to steady in their respective commoving reference frames. Thus, we begin our discussion using model results from day 31 of the integration. The phase speed of northward propagation in the initial problem can be calculated by the slope of precipitation at the date line in the Northern Hemisphere.

The zonally averaged SST, as well as the vertical gradient of mean moisture $\tilde{Q}$, is assumed to be maximum at the equator, which has a meridional structure of $\exp[-(y/y_L)^2]$. We use $y_L = 30°$ in accordance with the observation (Kang et al. 2013). The CMT will be controlled by the seasonal-mean VWS U, which is assumed to have a structure of

$$U = U_0 \exp\{-[(y - y_0)/y_s]^2\}, \tag{5}$$

which has a meridional scale of $y_s = 15°$. The magnitude is denoted by U_0, and y_0 is the center of the profile. To isolate the role of asymmetric CMT, the SST is assumed to be equatorially trapped, and the northward propagation of ISO due to the subtropical maximum SST is prohibited.

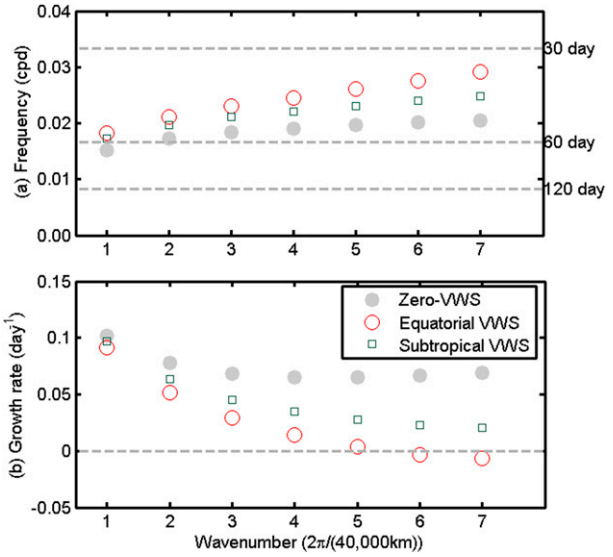

FIG. 2. Roles of CMT represented by the eigenvalues under different VWSs. (a) Frequency and (b) growth rate, drawn for the experiments with zero VWS ($U_0 = 0\,\mathrm{m\,s^{-1}}$), equatorially trapped easterly VWS ($U_0 = -15\,\mathrm{m\,s^{-1}}$ and $y_0 = 0$), and subtropical easterly VWS ($U_0 = -15\,\mathrm{m\,s^{-1}}$ and $y_0 = 10°\mathrm{N}$). Here, zero momentum and thermal damping of $d = 0$ are used. The VWSs are zonally symmetric and have a meridional structure defined in Eq. (5).

3. Role of CMT under different VWSs: Analytical solution

Figure 2 shows the eigenvalues for different VWS structures. Without the VWS and its associated CMT, this model gives a peculiar dispersion relation and selects the longest eastward-propagating mode as the most unstable mode. This is inconsistent with the results of Liu and Wang where only the baroclinic mode and the PBL process are coupled (Liu and Wang 2012a). When the easterly VWS is included, the CMT accelerates the eastward propagation of eastward-propagating modes and reduces the instability, especially for the short waves. The CMT under the equatorially trapped easterly VWS seems to act more efficiently to accelerate the eastward propagation than the subtropical easterly VWS does. These results are reversed under the westerly VWS (not shown). This finding is based on the theoretical model, and the mechanism of CMT reducing the frictional convergence instability should be further studied by GCM experiments in the future.

Without the VWS, the strong positive equatorial temperature anomalies are sandwiched by negative

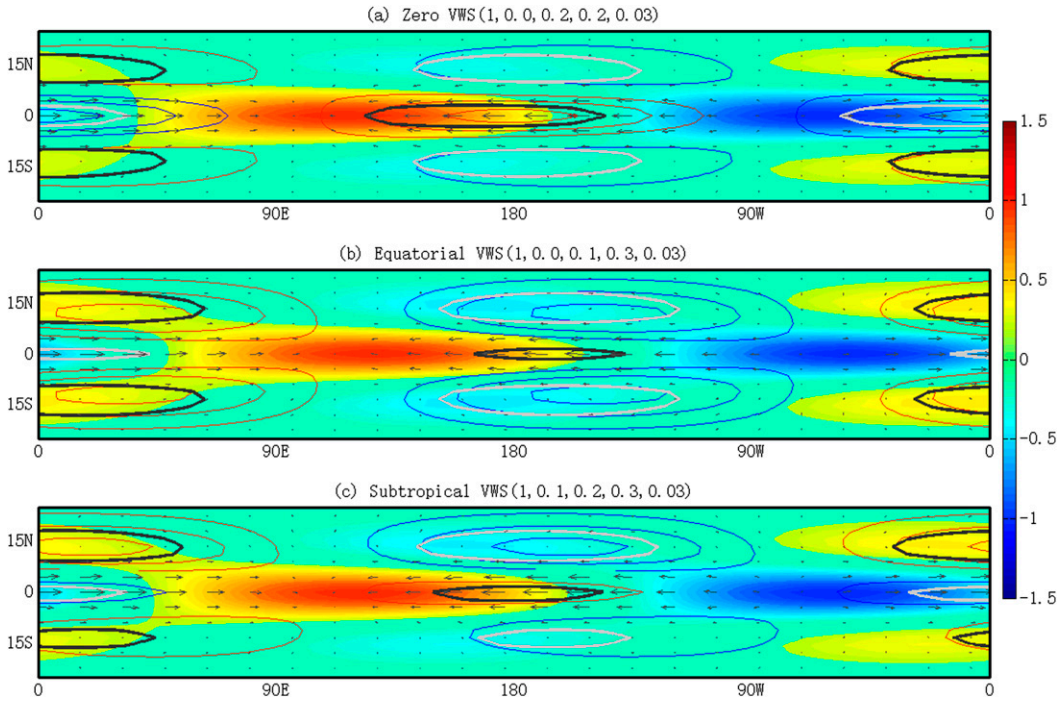

FIG. 3. Eigenvectors of unstable modes corresponding to wavenumber 1 in Fig. 2. Normalized lower-level velocity vectors, precipitation (shading), with temperature anomalies (contours) of experiments under (a) zero VWS, (b) equatorially trapped easterly VWS, and (c) subtropical easterly VWS are drawn for eastward wavenumber 1. Positive (negative) contours are denoted by red (blue). The contour interval is one-third of the magnitude, and zero contours are not drawn. Dark (gray) thick lines indicate that the upward (downward) Ekman pumping magnitude is 0.7. The five values in the brackets denote the magnitudes of zonal wind, meridional wind, temperature, precipitation, and Ekman pumping, respectively.

subtropical temperature anomalies in front of positive convective center, and the strong upward equatorial Ekman pumping is excited there (Fig. 3a). Thus, the PBL will pump additional moisture into the free troposphere to sustain the growth of eastward-propagating modes. In this model the PBL moisture convergence is maximum at the equator and decays poleward, which favors the growth of the Kelvin waves rather than the Rossby waves, thus the Rossby component and its cyclonic winds are relatively weak.

Without the PBL, the baroclinic eddy momentum transport from synoptic-scale motions can provide an instability source for the MJO (Liu and Wang 2013). Here, the barotropic CMT by cumulus convection will reduce the instability from the PBL moisture convergence, and this negative role of the barotropic CMT is stronger for shorter waves (Fig. 2b), which can be explained by analyzing the horizontal structures. Because of the coupling of equatorial Rossby waves and Kelvin waves (Wang and Rui 1990), the equatorial upward Ekman pumping is sandwiched by subtropical downward Ekman pumping in front of the positive convective center (Fig. 3a). The inclusion of CMT under the equatorially trapped easterly VWS will accelerate the zonal wind and enhance the subtropical gyre through the geostrophic balance, which enhances the subtropical downward Ekman pumping and suppresses the equatorial upward Ekman pumping (Fig. 3b). The subtropical gyre affected by the CMT is stronger for shorter waves. This is because the temperature-anomaly-induced Ekman pumping is much stronger in the subtropics than that at the equator for short waves (Liu and Wang 2012a). Thus, in front of the convective center, the equatorial upward Ekman pumping is greatly reduced for short waves (Fig. 4), and the PBL-pumped moisture for the growth of short waves is reduced by the inclusion of CMT under easterly VWS.

It is interesting that the CMT under the subtropical VWS excites asymmetric structure and the precipitation is enhanced in the Northern Hemisphere (Fig. 3c). Under the easterly VWS of Asian summer monsoon, the CMT is much stronger in the Northern Hemisphere than in the Southern Hemisphere. The simulated temperature anomalies in the Northern Hemisphere are strong, as well as the Ekman-pumping-induced precipitation. The strong positive Ekman pumping to the northwest of positive

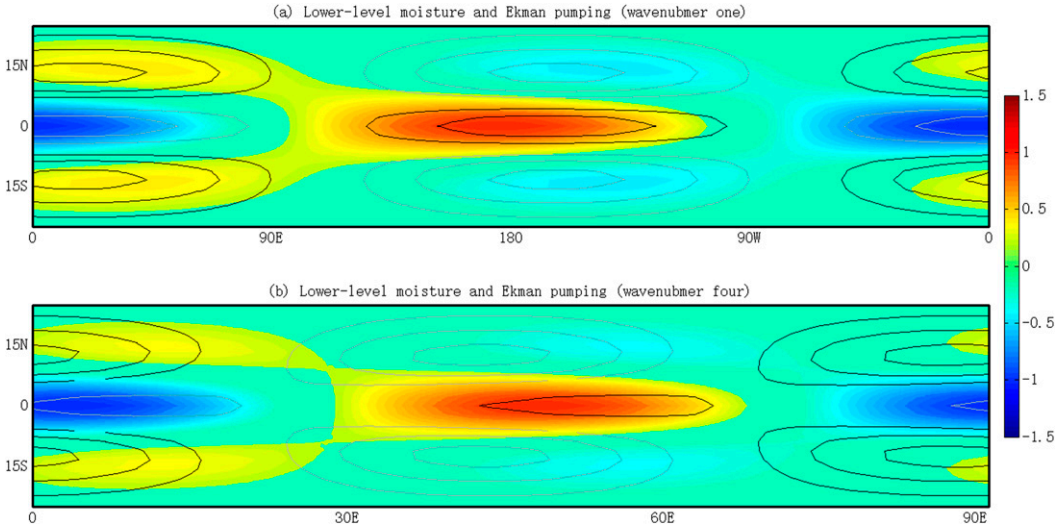

FIG. 4. Relationship between moisture and Ekman pumping of unstable modes in Fig. 2. Normalized lower-level moisture anomalies (shading), with Ekman pumping (contour) of experiments under equatorial easterly VWS for (a) wavenumber 1 and (b) wavenumber 4. Dark (gray) thick lines denote the upward (downward) Ekman pumping. The contour interval is one-third of the magnitude, and zero contours are not drawn.

precipitation region contributes to this asymmetric structure. Since this zonal wavenumber–frequency projection cannot represent the northward propagation of perturbation, it is necessary to integrate this model from an initial perturbation and see how this perturbation evolves.

4. Role of CMT under different VWSs: Initial value problem

Figure 5a shows the model evolution from an initial wavenumber-1 Kelvin wave–like disturbance maximum at the equator, which has a horizontal structure of $\exp(-y^2/2)\sin(2\pi x/L)$, where L is the nondimensional circumference at the equator. Under the easterly VWS of Asian summer monsoon, a northwest–southeast-tilted rainband is simulated. A robust northward propagation causes this tilt. The simulated northward propagation has a phase speed of $0.77°\,\text{day}^{-1}$, which is inconsistent with the observed $0.75°\,\text{day}^{-1}$ of the BSISO over the Indian Ocean (K10). In Fig. 5a, positive precipitation near the equator is accompanied by negative precipitation to its north. The CMT, in phase with the precipitation under the easterly VWS, produces a meridional dipolelike wind tendency spanning this dipole precipitation structure, which excites upward Ekman pumping to the north of the positive convective center. The moisture pumped by this Ekman pumping enhances the precipitation to the north of the original precipitation and induces the northward propagation. Although the initial perturbation has a Kelvin wave–like structure, this model under the asymmetric easterly VWS selects the Rossby wave–like mode as the fastest growing mode.

As noted by many previous works, the barotropic vorticity effect is the dominant mechanism for the northward propagation of the BSISO (Jiang et al. 2004; DeMott et al. 2013). The CMT under the easterly VWS of Asian monsoon also tends to accelerate the barotropic vorticity to the north of the BSISO convective center, which favors the northward propagation of the BSISO through exciting the upward Ekman pumping.

In Fig. 5a, the strong precipitation centered in the monsoon region will also initiate precipitation with a negative phase near the equatorial region through local self-initiated mechanism (Jiang and Li 2005; Wang et al. 2005; Liu and Wang 2012c). Thus, the oscillation period of the BSISO is determined by the phase speed of northward propagation. In this simple theoretical model, the northward propagation speed is parameter dependent. In Table 1, we show that strong easterly VWS will increase the CMT and accelerate the northward propagation as well. The northward propagation caused by the CMT is steady with respect to the PBL friction E, and sensitivity experiments showed that when the PBL friction changes from 0.5 day to 1 day, the northward propagation speed is only decreased by $0.05°\,\text{day}^{-1}$.

The northward propagation also depends on the location of the easterly VWS (Fig. 5). When the easterly VWS is symmetric about the equator (Fig. 5c), it excites symmetric positive Ekman pumping to both sides of the equatorial precipitation, and the model still simulates

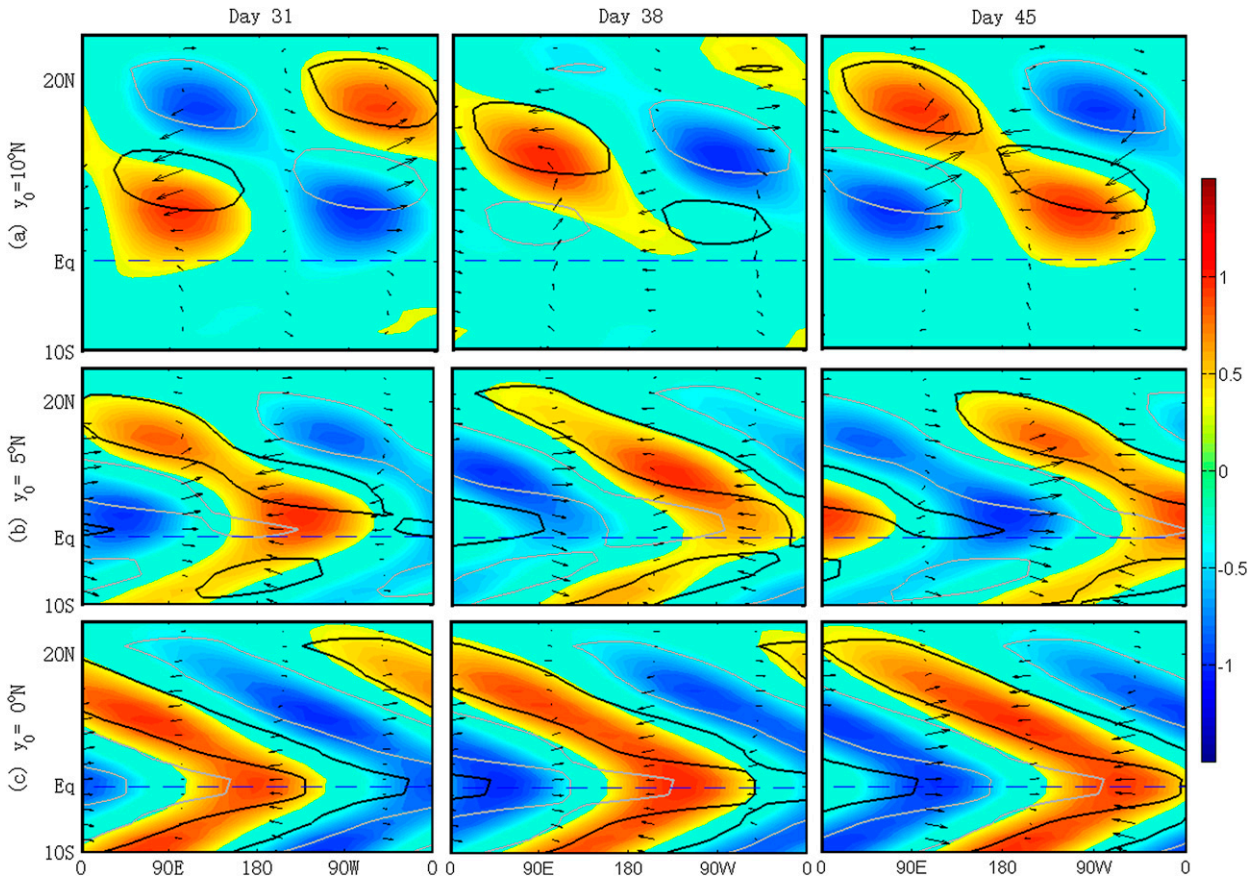

FIG. 5. Model evolution initiated from an equatorial wavenumber-1 Kelvin wave–like disturbance under different easterly VWSs. Normalized lower-level velocity vector, precipitation (shading) and Ekman pumping (contour) are drawn from days 31 to 45 for different experiments under easterly VWS, with its center at (a) the monsoon region $y_0 = 10°$N, (b) the subtropics $y_0 = 5°$N, and (c) the equator $y_0 = 0°$. Dark (gray) contours denote upward (downward) Ekman pumping that has a value of one-third of the magnitude. The VWSs are zonally symmetric and have a meridional structure defined in Eq. (5) and a magnitude of $U_0 = -15\,\mathrm{m\,s^{-1}}$.

the Gill-like pattern (Gill 1980), although the subtropical signal is enhanced. When the mean easterly VWS moves to the Northern Hemisphere and $y_0 = 5°$N (Fig. 5b), this symmetry is destroyed and a southeast–northwest-tilted rainband is simulated. Because the CMT and excited Ekman pumping in the Northern Hemisphere are stronger than those in the Southern Hemisphere, the enhanced subtropical Rossby waves emanating from the eastward-propagation forms this tilted rainband (Wang and Xie 1997; Lawrence and Webster 2002; Hsu et al. 2004). The northward propagation of the rain belt is evident in both cases (Figs. 5b,c), and the subtropical VWS also accelerates the eastward propagation by decreasing the equatorial upward Ekman pumping and growth rate. The eastward-propagation speeds of simulated modes under the equatorial and subtropical VWS are 9.7 and 12.0 $\mathrm{m\,s^{-1}}$, respectively, and modes with subtropical VWS have fast phase speed. This result is different from that of Fig. 2, in which no meridional propagation exists and modes with equatorial VWS have fast phase speed. Associated with the strong northward propagation, the eastward propagation is very fast (Fig. 5a). When the VWS is maximum at 5°N, the weak northward propagation also accelerates the eastward propagation (Fig. 5b). When the easterly VWS moves farther north of $y_0 = 10°$N (Fig. 5a), this

TABLE 1. Simulated phase speed of northward propagation as a function of easterly VWS magnitude U_0.

U_0 ($\mathrm{m\,s^{-1}}$)	−5	−10	−15	−20	−25
Phase speed of northward propagation (° $\mathrm{day^{-1}}$)	0.43	0.57	0.77	0.85	1.0

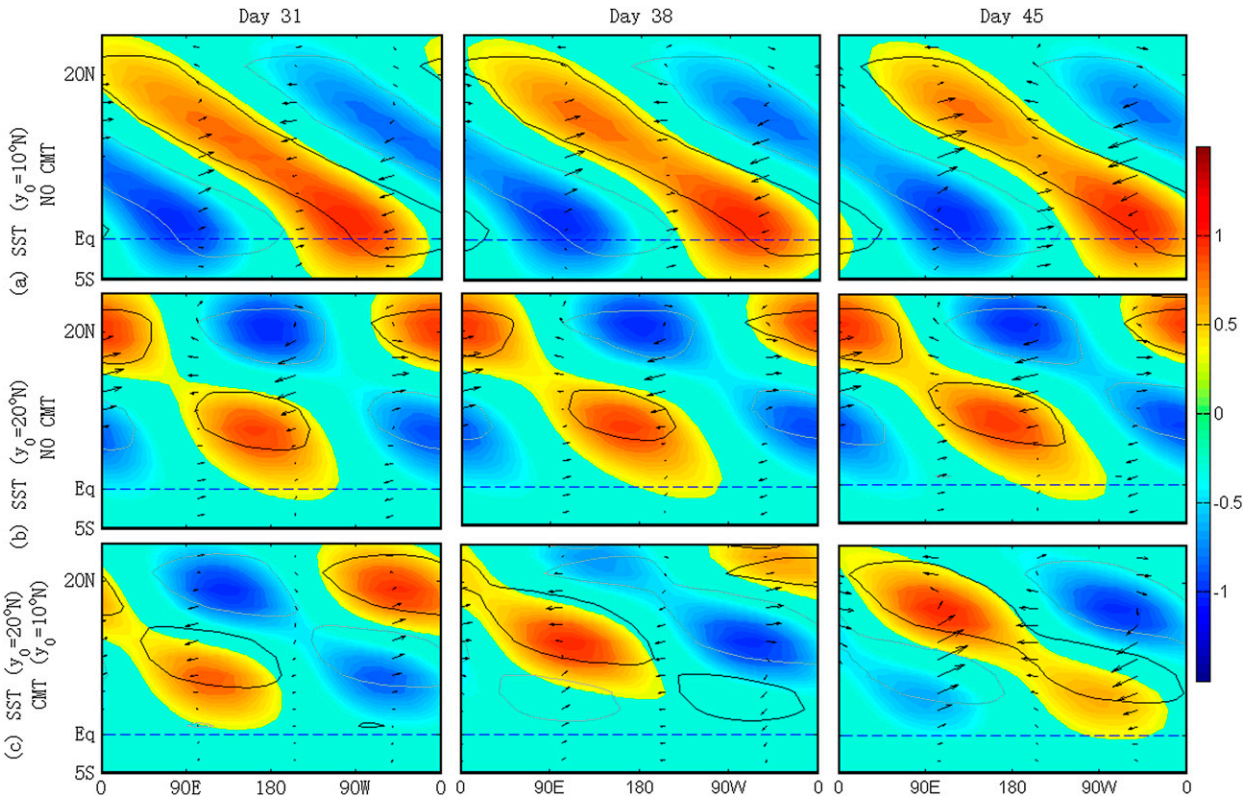

FIG. 6. Model evolution initiated from an equatorial wavenumber-1 Kelvin wave–like disturbance under different easterly VWS and SST. Normalized lower-level velocity vector, precipitation (shading), and Ekman pumping (contour) are drawn from days 31 to 45 for different experiments with subtropical SST centered at (a) 10°N and (b) 20°N. No VWS is included in these two experiments. (c) As in (a) and (b), but that the subtropical SST is centered at 20°N and the easterly VWS is centered at y_0 = 10°N is also included. Dark (gray) contours denote upward (downward) Ekman pumping that has a value of one-third of the magnitude. The VWSs are zonally symmetric and have a meridional structure defined in Eq. (5) and a magnitude of $U_0 = -15\,\mathrm{m\,s^{-1}}$.

model is dominated by the northward propagation of perturbation. Because the CMT and its Ekman pumping reach their maxima at 10°N, they produce strong precipitation to the north of the equatorial precipitation and the dominant northward propagation appears.

In boreal summer, the maximum SST is located at 20°N over the northern Indian Ocean. This asymmetric SST prefers enhancing the Rossby wave component of the ISO (Kang et al. 2013; Liu et al. 2015), because the time-mean intertropical convergence zone (ITCZ) is set by the SST and is located away from the equator (Lindzen and Nigam 1987; Sobel 2007). To compare the roles of the asymmetric SST and CMT in the BSISO, sensitivity experiments with maximum SST in the subtropics or at the equator are carried out (Fig. 6), and the SST structures and amplitudes are the same as other experiments. When the maximum SST moves northward, the Rossby wave component is enhanced (Figs. 6a,b), which is inconsistent with the theoretical results (Kang et al. 2013; Liu et al. 2015). Over this asymmetric SST, the northward propagation is simulated. The SST-induced northward propagation, however, is mainly caused by the Rossby wave emanation mechanism (Wang and Xie 1997; Lawrence and Webster 2002). This northward-propagation speed, with values below $0.2°\,\mathrm{day^{-1}}$, is determined by the eastward propagation of the simulated signal and is slow compared to the observed northward propagation of about $0.75°\,\mathrm{day^{-1}}$. When the subtropical CMT is also included, a significant northward propagation with a speed of $0.65°\,\mathrm{day^{-1}}$ is simulated (Fig. 6c). These experiments mean that in this simple model, the barotropic CMT is more sufficient in inducing the northward propagation of ISO than the asymmetric SST.

5. Conclusions

Recent multimodel analysis of the MJO revealed that the coupling of PBL moisture convergence and free-tropospheric convection may be important for MJO simulation, which means that the instability from the PBL is important for understanding the ISO (Jiang et al.

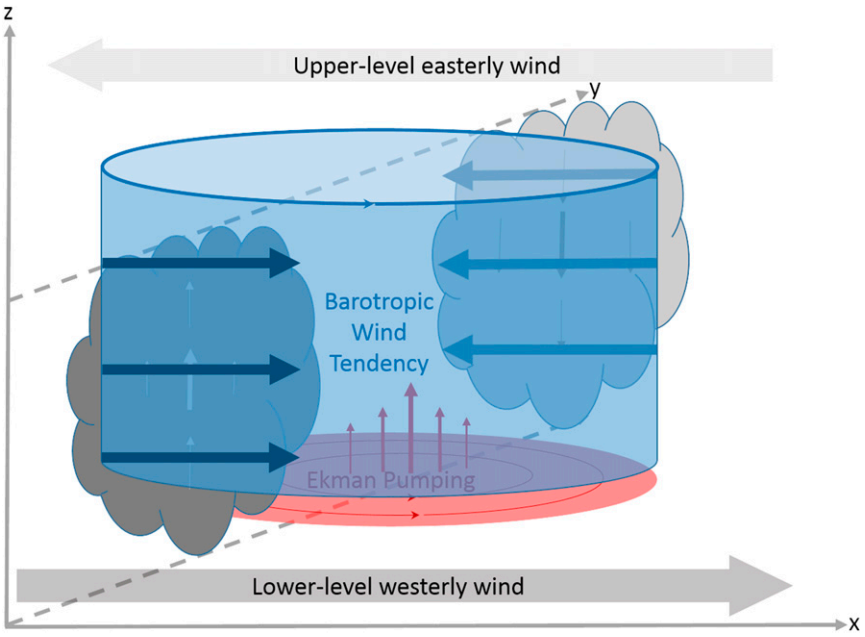

FIG. 7. Schematic diagram showing the mechanism for the generation of upward Ekman pumping to the north of the BSISO due to barotropic CMT. Dark (gray) clouds denote the positive (negative) convection of BSISO, and the broad blue arrows denote barotropic CMT. The red upward arrows denote upward Ekman pumping due to the cyclonic barotropic CMT.

2015). Under the easterly VWS, the CMT will suppress the instability induced by PBL moisture convergence and accelerate the eastward propagation, especially for short waves; this is the new mechanism we use to explain why the MJO prefers the planetary scale. We view examination of this scale-selection mechanism in GCMs as a target for future study.

This work also presents that the CMT by cumulus convection can induce the northward propagation of the BSISO through exciting the barotropic vorticity to the north of the BSISO. Figure 7 summarizes this mechanism for the generation of upward Ekman pumping to the north of the BSISO due to barotropic CMT. Under the easterly VWS of Asian summer monsoon, the CMT caused by positive convection of the BSISO tends to accelerate the barotropic westerly wind. The negative convection or downward motion to the north of this BSISO, however, is going to accelerate the barotropic easterly wind. Thus, a positive barotropic vorticity tendency is induced to the north of the BSISO convective center, which should excite upward Ekman pumping and prepare enough moisture for the northward propagation of the BSISO. The mechanism behind possible CMT impact on the northward propagation described in this study is different from that in K10. K10 stressed the importance of the baroclinic secondary circulation induced by cumulus friction, which results in lower-tropospheric convergence to the north of convection; their simulated northward propagation, however, is too weak compared to the observation. This study emphasizes the importance of the barotropic CMT for the northward propagation of the BSISO.

In this paper, we only focused on the role of the CMT and neglected another important mechanism for the northward propagation of the ISO, the vertical shear mechanism proposed by Jiang et al. (Jiang et al. 2004) and Drbohlav and Wang (Drbohlav and Wang 2005). They argued that the generation of barotropic vorticity due to coupling between atmospheric baroclinic and barotropic modes in the presence of vertical shear in the mean flow causes moisture convergence in the PBL, which leads to the northward shift of convection. This barotropic vorticity can also be effectively generated by the upward transport of westerly momentum by cumulus convection over the Indian monsoon region during the boreal summer. In future, these two mechanisms should be compared using the same model by adding both the advection and CMT terms.

In recent global 7-km cloud-resolving model simulation (Miyakawa et al. 2012) and observation analysis based on the NOAA/Climate Forecast System Reanalysis (CFSR) (Oh et al. 2015), the CMT showed a 3-layer structure: positive momentum tendency anomalies near the surface, negative (positive) in the lower to midtroposphere, and strong positive (negative) in the

upper troposphere were found within and to the west (to the east) of the MJO convection. This means CMT not only has the barotropic mode but also has a baroclinic mode. Over the convective center, the baroclinic CMT should accelerate the lower-tropospheric easterly wind and produce anticyclonic wind anomalies to the north of the convective center, which may be a *negative* feedback in the northward propagation of BSISO. The observed positive PBL CMT and positive barotropic CMT in convective center supports our strong barotropic mode assumption. In this paper, we focused on demonstrating the role of the barotropic CMT. A more realistic 3-layer vertical structure, instead of this simple 2-layer model, should be tested in the future.

These results imply that accurate simulation of the mean state in the GCM is important to capture the realistic CMT by cumulus convection, which is important for ISO simulation. In a recent study (Hung et al. 2013), the improved tropical intraseasonal variability in two Coupled Model Intercomparison Project phase 5 (CMIP5) models with CMT included (i.e., CCSM4 and CNRM-CM5) as compared to their CMIP3 versions suggests the potential importance of CMT (Yukimoto et al. 2012; Zhou et al. 2012). The role of CMT in the ISO should be further studied in more CMIP5 models.

Acknowledgments. We are grateful for helpful and encouraging comments from three anonymous reviewers and Chongyin Li. This work was supported by China National 973 Project 2015CB453200, the NOAA/MAPP project (under Award NA10OAR4310247), the Asian-Pacific Economic Cooperation (APEC) Climate Center, and the National Research Foundation (NRF) of Korea through a Global Research Laboratory (GRL) Grant (MEST, 2011-0021927). In-Sik Kang was supported by the National Research Foundation of Korea Grant (MEST) (NRF-2012M1A2A2671775) and the BK21 program.

REFERENCES

Annamalai, H., and J. Slingo, 2001: Active/break cycles: Diagnosis of the intraseasonal variability of the Asian Summer Monsoon. *Climate Dyn.,* **18,** 85–102, doi:10.1007/s003820100161.

——, and K. Sperber, 2005: Regional heat sources and the active and break phases of boreal summer intraseasonal (30–50 day) variability. *J. Atmos. Sci.,* **62,** 2726–2748, doi:10.1175/JAS3504.1.

Boos, W. R., and Z. Kuang, 2010: Mechanisms of poleward propagating, intraseasonal convective anomalies in cloud system-resolving models. *J. Atmos. Sci.,* **67,** 3673–3691, doi:10.1175/2010JAS3515.1.

DeMott, C. A., C. Stan, and D. A. Randall, 2013: Northward propagation mechanisms of the boreal summer intraseasonal oscillation in the ERA-Interim and SP-CCSM. *J. Climate,* **26,** 1973–1992, doi:10.1175/JCLI-D-12-00191.1.

Drbohlav, H.-K. L., and B. Wang, 2005: Mechanism of the northward-propagating intraseasonal oscillation: Insights from a zonally symmetric model. *J. Climate,* **18,** 952–972, doi:10.1175/JCLI3306.1.

Frierson, D. M., A. J. Majda, and O. M. Pauluis, 2004: Large scale dynamics of precipitation fronts in the tropical atmosphere: A novel relaxation limit. *Commun. Math. Sci.,* **2,** 591–626, doi:10.4310/CMS.2004.v2.n4.a3.

Gill, A. E., 1980: Some simple solutions for heat-induced tropical circulation. *Quart. J. Roy. Meteor. Soc.,* **106,** 447–462, doi:10.1002/qj.49710644905.

Gyoswami, B., and J. Shukla, 1984: Quasi-periodic oscillations in a symmetric general circulation model. *J. Atmos. Sci.,* **41,** 20–37, doi:10.1175/1520-0469(1984)041<0020:QPOIAS>2.0.CO;2.

Hsu, H.-H., C.-H. Weng, and C.-H. Wu, 2004: Contrasting characteristics between the northward and eastward propagation of the intraseasonal oscillation during the boreal summer. *J. Climate,* **17,** 727–743, doi:10.1175/1520-0442(2004)017<0727:CCBTNA>2.0.CO;2.

Hsu, P.-c., and T. Li, 2012: Role of the boundary layer moisture asymmetry in causing the eastward propagation of the Madden–Julian oscillation. *J. Climate,* **25,** 4914–4931, doi:10.1175/JCLI-D-11-00310.1.

Hung, M.-P., J.-L. Lin, W. Wang, D. Kim, T. Shinoda, and S. J. Weaver, 2013: MJO and convectively coupled equatorial waves simulated by CMIP5 climate models. *J. Climate,* **26,** 6185–6214, doi:10.1175/JCLI-D-12-00541.1.

Jiang, X., and T. Li, 2005: Reinitiation of the boreal summer intraseasonal oscillation in the tropical Indian Ocean. *J. Climate,* **18,** 3777–3795, doi:10.1175/JCLI3516.1.

——, ——, and B. Wang, 2004: Structures and mechanisms of the northward propagating boreal summer intraseasonal oscillation. *J. Climate,* **17,** 1022–1039, doi:10.1175/1520-0442(2004)017<1022:SAMOTN>2.0.CO;2.

——, and Coauthors, 2015: Vertical structure and diabatic processes of the Madden–Julian Oscillation: Exploring key model physics in cimate simulations. *J. Geophys. Res.,* doi:10.1002/2014JD022375, in press.

Kanamitsu, M., W. Ebisuzaki, J. Woollen, S.-K. Yang, J. Hnilo, M. Fiorino, and G. Potter, 2002: NCEP–DOE AMIP-II Reanalysis (R-2). *Bull. Amer. Meteor. Soc.,* **83,** 1631–1643, doi:10.1175/BAMS-83-11-1631.

Kang, I.-S., and I. M. Held, 1986: Linear and nonlinear diagnostic models of stationary eddies in the upper troposphere during northern summer. *J. Atmos. Sci.,* **43,** 3045–3057, doi:10.1175/1520-0469(1986)043<3045:LANDMO>2.0.CO;2.

——, D. Kim, and J.-S. Kug, 2010: Mechanism for northward propagation of boreal summer intraseasonal oscillation: Convective momentum transport. *Geophys. Res. Lett.,* **37,** L24804, doi:10.1029/2010GL045072.

——, F. Liu, M.-S. Ahn, Y.-M. Yang, and B. Wang, 2013: The role of SST structure in convectively coupled Kelvin–Rossby waves and its implications for MJO formation. *J. Climate,* **26,** 5915–5930, doi:10.1175/JCLI-D-12-00303.1.

Kemball-Cook, S., and B. Wang, 2001: Equatorial waves and air–sea interaction in the boreal summer intraseasonal oscillation. *J. Climate,* **14,** 2923–2942, doi:10.1175/1520-0442(2001)014<2923:EWAASI>2.0.CO;2.

Khouider, B., and A. J. Majda, 2006: A simple multicloud parameterization for convectively coupled tropical waves. Part I: Linear analysis. *J. Atmos. Sci.,* **63,** 1308–1323, doi:10.1175/JAS3677.1.

——, and ——, 2007: A simple multicloud parameterization for convectively coupled tropical waves. Part II: Nonlinear simulations. *J. Atmos. Sci.,* **64,** 381–400, doi:10.1175/JAS3833.1.

Kikuchi, K., and Y. N. Takayabu, 2004: The development of organized convection associated with the MJO during TOGA COARE IOP: Trimodal characteristics. *Geophys. Res. Lett.,* **31,** L10101, doi:10.1029/2004GL019601.

——, B. Wang, and Y. Kajikawa, 2012: Bimodal representation of the tropical intraseasonal oscillation. *Climate Dyn.,* **38,** 1989–2000, doi:10.1007/s00382-011-1159-1.

Kiladis, G. N., K. H. Straub, and P. T. Haertel, 2005: Zonal and vertical structure of the Madden–Julian Oscillation. *J. Atmos. Sci.,* **62,** 2790–2809, doi:10.1175/JAS3520.1.

Lawrence, D. M., and P. J. Webster, 2002: The boreal summer intraseasonal oscillation: Relationship between northward and eastward movement of convection. *J. Atmos. Sci.,* **59,** 1593–1606, doi:10.1175/1520-0469(2002)059<1593:TBSIOR>2.0.CO;2.

Li, T., and C. Zhou, 2009: Planetary scale selection of the Madden–Julian oscillation. *J. Atmos. Sci.,* **66,** 2429–2443, doi:10.1175/2009JAS2968.1.

Lindzen, R. S., and S. Nigam, 1987: On the role of sea surface temperature gradients in forcing low-level winds and convergence in the tropics. *J. Atmos. Sci.,* **44,** 2418–2436, doi:10.1175/1520-0469(1987)044<2418:OTROSS>2.0.CO;2.

Liu, F., and B. Wang, 2012a: A frictional skeleton model for the Madden–Julian oscillation. *J. Atmos. Sci.,* **69,** 2749–2758, doi:10.1175/JAS-D-12-020.1.

——, and ——, 2012b: A model for the interaction between 2-day waves and moist Kelvin waves. *J. Atmos. Sci.,* **69,** 611–625, doi:10.1175/JAS-D-11-0116.1.

——, and ——, 2012c: A conceptual model for self-sustained active-break Indian summer monsoon. *Geophys. Res. Lett.,* **39,** L20814, doi:10.1029/2012GL053663.

——, and ——, 2013: Impacts of upscale heat and momentum transfer by moist Kelvin waves on the Madden–Julian oscillation: A theoretical model study. *Climate Dyn.,* **40,** 213–224, doi:10.1007/s00382-011-1281-0.

——, G. Huang, and Y. Mi, 2015: Role of SST meridional structure in coupling the Kelvin and Rossby waves of the intraseasonal oscillation. *Theor. Appl. Climatol.,* doi:10.1007/s00704-014-1266-0, in press.

Madden, R. A., 1986: Seasonal variations of the 40–50 day oscillation in the tropics. *J. Atmos. Sci.,* **43,** 3138–3158, doi:10.1175/1520-0469(1986)043<3138:SVOTDO>2.0.CO;2.

——, and P. R. Julian, 1971: Detection of a 40–50 day oscillation in the zonal wind in the tropical Pacific. *J. Atmos. Sci.,* **28,** 702–708, doi:10.1175/1520-0469(1971)028<0702:DOADOI>2.0.CO;2.

——, and ——, 1972: Description of global-scale circulation cells in the tropics with a 40–50 day period. *J. Atmos. Sci.,* **29,** 1109–1123, doi:10.1175/1520-0469(1972)029<1109:DOGSCC>2.0.CO;2.

——, and ——, 1994: Observations of the 40–50-day tropical oscillation—A review. *Mon. Wea. Rev.,* **122,** 814–837, doi:10.1175/1520-0493(1994)122<0814:OOTDTO>2.0.CO;2.

Majda, A. J., and J. A. Biello, 2004: A multiscale model for tropical intraseasonal oscillations. *Proc. Natl. Acad. Sci. USA,* **101,** 4736–4741, doi:10.1073/pnas.0401034101.

——, and S. N. Stechmann, 2009: The skeleton of tropical intraseasonal oscillations. *Proc. Natl. Acad. Sci. USA,* **106,** 8417–8422, doi:10.1073/pnas.0903367106.

Miyakawa, T., Y. N. Takayabu, T. Nasuno, H. Miura, M. Satoh, and M. W. Moncrieff, 2012: Convective momentum transport by rainbands within a Madden–Julian oscillation in a global nonhydrostatic model with explicit deep convective processes. Part I: Methodology and general results. *J. Atmos. Sci.,* **69,** 1317–1338, doi:10.1175/JAS-D-11-024.1.

Moore, A. M., and R. Kleeman, 1999: Stochastic forcing of ENSO by the intraseasonal oscillation. *J. Climate,* **12,** 1199–1220, doi:10.1175/1520-0442(1999)012<1199:SFOEBT>2.0.CO;2.

Mori, M., and M. Watanabe, 2008: The growth and triggering mechanisms of the PNA: A MJO-PNA coherence. *J. Meteor. Soc. Japan,* **86,** 213–236, doi:10.2151/jmsj.86.213.

Murakami, M., 1984: Analysis of the deep convective activity over the Western Pacific and Southeast Asia. II: Seasonal and intraseasonal variations during Northern Summer. *J. Meteor. Soc. Japan,* **62,** 88–108.

Myers, D. S., and D. E. Waliser, 2003: Three-dimensional water vapor and cloud variations associated with the Madden–Julian Oscillation during Northern Hemisphere winter. *J. Climate,* **16,** 929–950, doi:10.1175/1520-0442(2003)016<0929:TDWVAC>2.0.CO;2.

Oh, J.-H., X. Jiang, D. Waliser, M. W. Moncrieff, and R. H. Johnson, 2015: Convective momentum transport associated with the Madden–Julian oscillation based on a reanalysis dataset. *J. Climate,* in press.

Salby, M. L., and H. H. Hendon, 1994: Intraseasonal behavior of clouds, temperature, and motion in the Tropics. *J. Atmos. Sci.,* **51,** 2207–2224, doi:10.1175/1520-0469(1994)051<2207:IBOCTA>2.0.CO;2.

Schneider, E. K., and R. S. Lindzen, 1976: A discussion of the parameterization of momentum exchange by cumulus convection. *J. Geophys. Res.,* **81,** 3158–3160, doi:10.1029/JC081i018p03158.

Sobel, A. H., 2007: Simple models of ensemble-averaged precipitation and surface wind, given the sea surface temperature. *The Global Circulation of the Atmosphere,* T. Schneider and A. H. Sobel, Eds., Princeton University Press, 219–251.

——, and E. Maloney, 2012: An idealized semi-empirical framework for modeling the Madden–Julian oscillation. *J. Atmos. Sci.,* **69,** 1691–1705, doi:10.1175/JAS-D-11-0118.1.

——, and ——, 2013: Moisture modes and the eastward propagation of the MJO. *J. Atmos. Sci.,* **70,** 187–192, doi:10.1175/JAS-D-12-0189.1.

Sperber, K. R., and H. Annamalai, 2008: Coupled model simulations of boreal summer intraseasonal (30–50 day) variability. Part 1: Systematic errors and caution on use of metrics. *Climate Dyn.,* **31,** 345–372, doi:10.1007/s00382-008-0367-9.

Tian, B., D. E. Waliser, E. J. Fetzer, B. H. Lambrigtsen, Y. L. Yung, and B. Wang, 2006: Vertical moist thermodynamic structure and spatial temporal evolution of the MJO in AIRS observations. *J. Atmos. Sci.,* **63,** 2462–2485, doi:10.1175/JAS3782.1.

Tung, W.-W., and M. Yanai, 2002a: Convective momentum transport observed during the TOGA COARE IOP. Part I: General features. *J. Atmos. Sci.,* **59,** 1857–1871, doi:10.1175/1520-0469(2002)059<1857:CMTODT>2.0.CO;2.

——, and ——, 2002b: Convective momentum transport observed during the TOGA COARE IOP. Part II: Case studies. *J. Atmos. Sci.,* **59,** 2535–2549, doi:10.1175/1520-0469(2002)059<2535:CMTODT>2.0.CO;2.

Wang, B., 1988: Dynamics of tropical low-frequency waves: An analysis of the moist Kelvin wave. *J. Atmos. Sci.,* **45,** 2051–2065, doi:10.1175/1520-0469(1988)045<2051:DOTLFW>2.0.CO;2.

——, and H. Rui, 1990: Dynamics of the coupled moist Kelvin–Rossby wave on an equatorial β-plane. *J. Atmos. Sci.,* **47,** 397–413, doi:10.1175/1520-0469(1990)047<0397:DOTCMK>2.0.CO;2.

——, and Y. Xue, 1992: Behavior of a moist Kelvin wave packet with nonlinear heating. *J. Atmos. Sci.,* **49,** 549–559, doi:10.1175/1520-0469(1992)049<0549:BOAMKW>2.0.CO;2.

——, and T. Li, 1993: A simple tropical atmosphere model of relevance to short-term climate variations. *J. Atmos. Sci.,* **50,** 260–284, doi:10.1175/1520-0469(1993)050<0260:ASTAMO>2.0.CO;2.

——, and ——, 1994: Convective interaction with boundary-layer dynamics in the development of a tropical intraseasonal system. *J. Atmos. Sci.,* **51,** 1386–1400, doi:10.1175/1520-0469(1994)051<1386:CIWBLD>2.0.CO;2.

——, and X. Xie, 1997: A model for the boreal summer intraseasonal oscillation. *J. Atmos. Sci.,* **54,** 72–86, doi:10.1175/1520-0469(1997)054<0072:AMFTBS>2.0.CO;2.

——, and F. Liu, 2011: A model for scale interaction in the Madden–Julian oscillation. *J. Atmos. Sci.,* **68,** 2524–2536, doi:10.1175/2011JAS3660.1.

——, P. J. Webster, and H. Teng, 2005: Antecedents and self-induction of active-break south Asian monsoon unraveled by satellites. *Geophys. Res. Lett.,* **32,** 4704, doi:10.1029/2004GL020996.

Webster, P. J., and J. R. Holton, 1982: Cross-equatorial response to middle-latitude forcing in a zonally varying basic state. *J. Atmos. Sci.,* **39,** 722–733, doi:10.1175/1520-0469(1982)039<0722:CERTML>2.0.CO;2.

Wu, X., and M. Yanai, 1994: Effects of vertical wind shear on the cumulus transport of momentum: Observations and parameterization. *J. Atmos. Sci.,* **51,** 1640–1660, doi:10.1175/1520-0469(1994)051<1640:EOVWSO>2.0.CO;2.

Yano, J.-I., and K. Emanuel, 1991: An improved model of the equatorial troposphere and its coupling with the stratosphere. *J. Atmos. Sci.,* **48,** 377–389, doi:10.1175/1520-0469(1991)048<0377:AIMOTE>2.0.CO;2.

Yasunari, T., 1979: Cloudiness fluctuations associated with the Northern Hemisphere summer monsoon. *J. Meteor. Soc. Japan,* **57,** 227–242.

Yukimoto, S., and Coauthors, 2012: A New Global Climate Model of the Meteorological Research Institute: MRI-CGCM3—Model description and basic performance (special issue on recent development on climate models and future climate projections). *J. Meteor. Soc. Japan,* **90A,** 23–64, doi:10.2151/jmsj.2012-A02.

Zhang, C., 2005: Madden–Julian Oscillation. *Rev. Geophys.,* **43,** RG2003, doi:10.1029/2004RG000158.

——, and M. Dong, 2004: Seasonality in the Madden–Julian Oscillation. *J. Climate,* **17,** 3169–3180, doi:10.1175/1520-0442(2004)017<3169:SITMO>2.0.CO;2.

Zhou, L., and I.-S. Kang, 2013: Influence of Convective Momentum Transport on Mixed Rossby–Gravity Waves: A Contribution to Tropical 2-Day Waves. *J. Atmos. Sci.,* **70,** 2467–2475, doi:10.1175/JAS-D-12-0300.1.

——, R. B. Neale, M. Jochum, and R. Murtugudde, 2012: Improved Madden–Julian oscillations with improved physics: The impact of modified convection parameterizations. *J. Climate,* **25,** 1116–1136, doi:10.1175/2011JCLI4059.1.

Zhou, S., and A. J. Miller, 2005: The interaction of the Madden–Julian Oscillation and the Arctic Oscillation. *J. Climate,* **18,** 143–159, doi:10.1175/JCLI3251.1.